

Role of Spin, Phonon and Plasmon Dynamics on Ferromagnetism in Cr doped 3C-SiC

Gyanti Prakash Moharana, Rahul Kothari
Indian Institute of Technology Madras, Chennai-600036

S.K. Singh
CSIR Innovation Center for Plasma Processing, IMMT Bhubaneswar - 751013

N. Harish Kumar*
Indian Institute of Technology Madras, Chennai - 600036

The defect induced magnetism has initiated a lot of interest in field of spintronics. In this regard, SiC is a promising material because of its unique properties under extreme conditions. Hence it will be very much interesting to investigate the interaction between defects and itinerant carrier in doped SiC for spintronics application. We report the structural stability and magnetic interaction in Cr doped 3C-SiC synthesized by Thermal Plasma Technique. The EPR spectrum of undoped 3C-SiC shows a sharp resonance line corresponding to $g = 2.00$ associated with the defects present in the system. Anomalous temperature evolution tendency of the relative intensity of EPR spectra can be attributed to magnetically correlated defects in the host matrix. For the first time we report the detailed quantitative analysis of X-band and Q-band EPR study in Cr doped 3C-SiC which reveals that Cr can be in multivalent state. The non monotonous variation of Longitudinal Mode (LO) of the Raman spectra has been explained based on the interaction between carriers and surface plasmon using Longitudinal optical plasmon coupling model (LOPC). The carrier density calculated by using LOPC fit with experimental data varies from 1.8×10^{15} to $4.2 \times 10^{17} \text{ cm}^{-3}$. Room temperature magnetic measurements exhibit ferromagnetic behavior with non-zero coercivity for all the samples up to 7 T field. We, for the first time, show the Curie temperature to be above 760 K. Quantitative analysis of magnetic interaction validates the applicability of Bound Magnetic Polaron Model (BMP) which probably arises from the exchange interaction of Cr^{3+} ions with related (Si, C) defects. The polaron density estimated from the BMP fit agrees well with the carrier density obtained from the line shape fitting of Raman spectra.

I. INTRODUCTION

For developing a potential spintronics device it is necessary to have a magnetic semiconductor which is compatible with existing electronics principles. But to make a semiconductor carrying magnetic properties is not easy. Inducing magnetic order in a semiconductor by a transition metal doping has been a trend since Dietl. et al predicted the room temperature ferromagnetism in wide band gap semiconductor i.e., Mn (5%) doped GaN and ZnO [1, 2]. But it turns out that none of these are room temperature ferromagnetic semiconductors. A recent report on intrinsic ferromagnetic order in Co doped TiO_2 has revived interest in dilute magnetic semiconductor DMS [3]. It is known that SiC is a potentially wonderful material for spintronics device on account of its unique properties under extreme conditions such as high breakdown voltage, low thermal conductivity and high thermal expansion coefficient and hence can be used for high temperature and high power electronics applications. Thus it is interesting to explore the possibility of inducing ferromagnetism by doping transition metal elements. Among the various transition metals explored for inducing magnetism in 3C-SiC, the Cr substitution for Si and its potential application for spintronics device is hardly explored. We dope Cr in 3C-SiC to check whether it is pos-

sible to induce long range magnetic order in the host matrix via a novel synthesis technique called carbothermal reduction of silica in rice husk using plasma reactor [4, 5]. We must emphasize that although there are some reports in the literature on Cr doped 3C-SiC single crystal, thin film and others, there are no reports on detailed quantitative analysis of magnetic interactions, and its temperature dependence [6–9] to the best of our knowledge. Detailed investigation was carried out to study the temperature dependence of X-band and Q-band Electron Paramagnetic resonance both in high as well as low temperature regimes. DC Magnetization, and temperature variation Raman spectroscopy were carried out to check the crystalline quality of the sample. Quantitative analysis of magnetization is done using Bound Magnetic Polaron (BMP) model and role of lattice defects such as Si/C vacancies along with carrier concentration of transition metal element is discussed in details. A good agreement between the theory and experimental data has been achieved while considering the coupling between Longitudinal Optical (LO) mode with Plasmon induced by the surface deformation potential due to doping of transition metal element. So the LO phonon behavior is largely affected by the Longitudinal Optical Plasmon Coupling (LOPC) present in the system. In this report, we study the role of carrier concentration and lattice defects in the system as a function of temperature.

II. EXPERIMENTAL TECHNIQUE

The Cr doped bulk SiC polycrystalline samples were prepared by carbothermal reduction method. Rice husk was mixed with appropriate amounts of Cr_2O_3 . The growth tem-

* nhk@iitm.ac.in

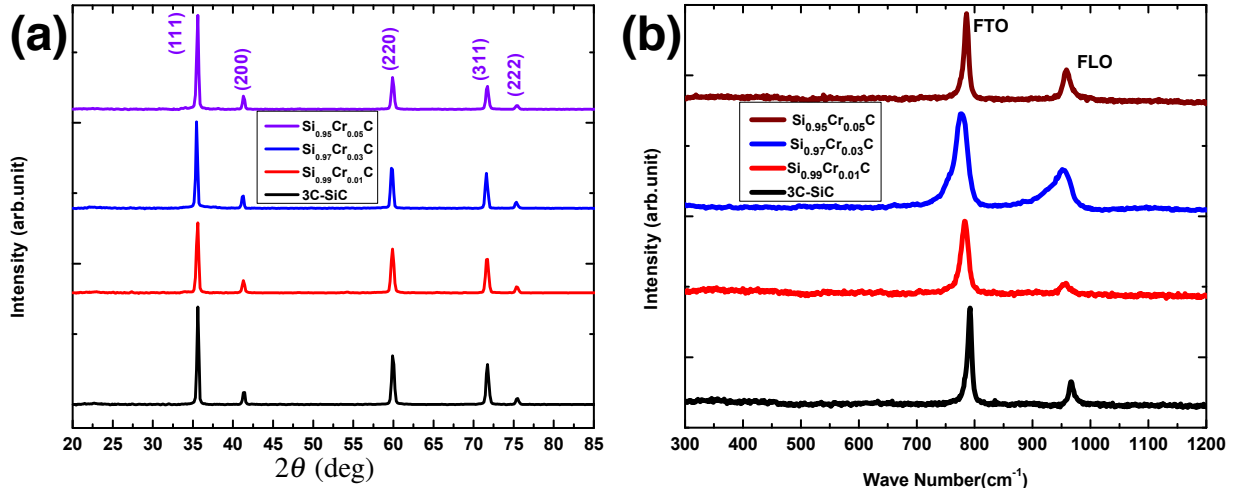


Figure 1. (a) X-Ray Diffraction pattern of undoped and Cr doped 3C-SiC shows the single phase nature of the samples. (b) Raman Spectra of undoped and Cr doped 3C-SiC at room temperature. It shows a clear shift and broadening of the spectra with increase in Cr concentration in the host matrix. This can be attributed to the incorporation of Cr in the pristine sample.

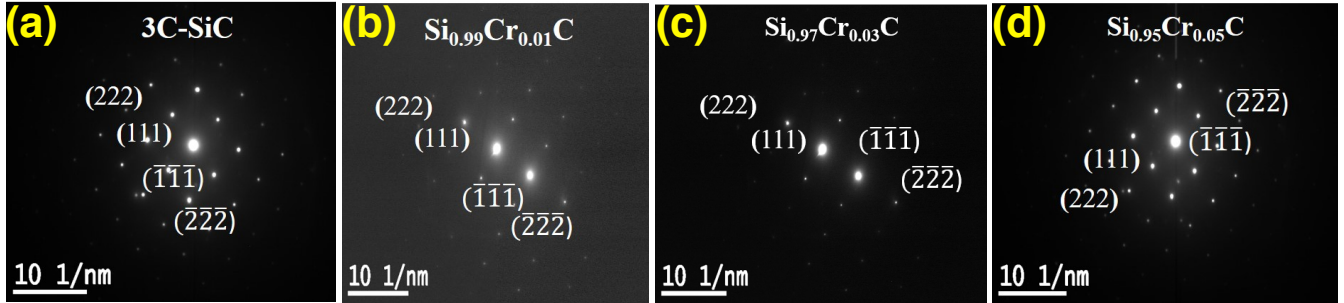
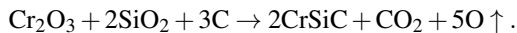


Figure 2. Transmission electron microscopy of undoped and Cr doped 3C-SiC. The figure clearly shows the four fold symmetry representing the cubic crystal structure preserved in both undoped and Cr doped 3C-SiC.

perature and time were fixed at 1600 °C and 15 mins respectively. The details of synthesis of SiC from rice husk can be found elsewhere [4]. Typical experimental conditions are Argon gas flow – 2 LPM; current – 50A, and load voltage – 300V. The possible reactions for the formation of SiC from Rice Husk can be written as



where as the chemical reaction for Cr incorporation in SiC is as follows



The structural characterization was carried out using Rigaku Smart lab X-ray diffractometer (XRD) with 9 kW power generator at room temperature and Horiba Jobin- Yvon HR-800 Micro Raman spectrometer with 488 nm laser wavelength. The quantum design SQUID-Vibrating Sample Magnetometer (VSM) was used to measure the magnetization at low temperature (5K -350K) up to 7 T. The high temperature measurements were carried out using a Lakeshore VSM. The valence state of unpaired electrons, dipolar interaction and anisotropy

in the system was probed using electron paramagnetic resonance spectrometer JEOL model JES FA 200. Fig. 1(a) shows the X-Ray diffraction pattern of undoped and Cr doped 3C-SiC. All diffraction peaks correspond to the cubic phase of SiC with symmetry group $F\bar{4}3m$. There was no signature of secondary phase of SiC or Cr oxide phase and Cr composite which indicates that Cr^{3+} cation replaces the Si^{4+} cation site in the 3C-SiC. It was found that the diffraction peaks of Cr doped SiC were shifted to lower angles and intensity was reduced in addition to an increase in Full Width at Half Maximum (FWHM). The corresponding expansion of the lattice parameter is expected because the ionic radius of dopant Cr^{3+} ion (0.52 Å) was larger than that of the host Si^{4+} (0.40 Å).

The average crystallite size of the Cr doped SiC was (determined by using Scherrer's formula) found to be < 100 nm. The Raman spectra of undoped and Cr doped 3C-SiC is shown in the Fig. 1(b). It clearly shows the variation of intensity and peak position with Cr concentrations. In order to get a better understanding of the systems, we use LOPC model to fit the experimental data (Temperature variation Raman spectra) and give the explanation for non monotonous variation of peak position and intensity of Raman spectra as a function of temper-

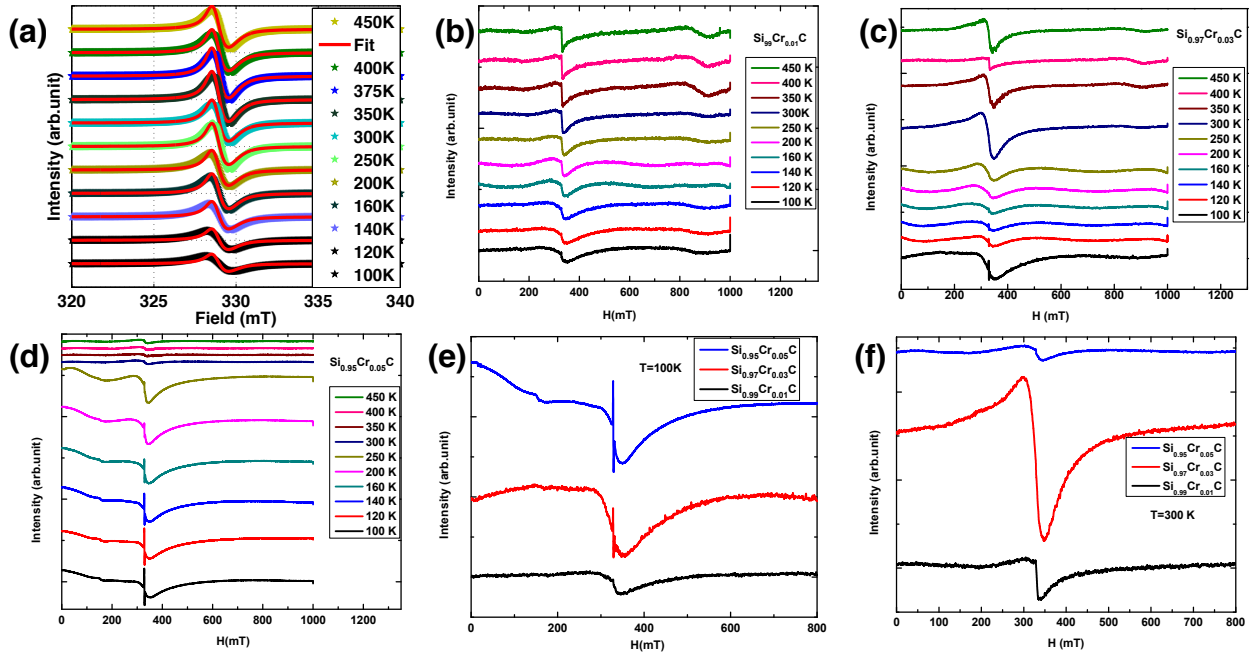


Figure 3. Temperature Variation of X-band Electron paramagnetic resonance of undoped and Cr doped 3C-SiC. Fig. (a) shows the temperature variation of EPR spectra of 3C-SiC. It clearly indicates an increase in intensity with an increase in temperature. Fig. (b, c, d) show Cr doped 3C-SiC. A sharp line along with a forbidden transition is an artifact of increase in Cr concentration. Fig. (e) shows a sharp line present in the spectrum which goes on decreasing with decrease in Cr concentration. In addition to this, there is a forbidden transition appearing in case of excess Cr doping in the system. Fig. (f) represents the effect of Cr concentration on EPR spectra at 300K. It shows that 3% Cr doped sample has more line width and intensity as compared to other two Cr (1%, & 5%).

ature and concentrations. Transmission electron microscopy selected area diffraction pattern (SAED) is shown in Fig. 2 which further confirms the crystalline quality of the samples.

III. ELECTRON PARAMAGNETIC RESONANCE

A. X Band EPR Spectra of Cr Doped 3C-SiC

Electron Paramagnetic Resonance (EPR) measurements were carried out using a JEOL X-band (frequency - 9.5 GHz) spectrometer using a rectangular cavity with 100 kHz field modulation and phase sensitive detection. The (EPR) absorption peaks for pure 3C-SiC are located around 329.05 mT, corresponding to $g = 2.00$ with the line width as narrow as 0.98 mT. This confirms the presence of vacancies in the host matrix [10, 11] as shown in the Fig. 3(a). In order to probe the nature of magnetic phase, spin dynamics, spin relaxation and internal field, the temperature variation of EPR is an effective tool. Fig. 3(a, b, c, d) shows the EPR spectra of doped and undoped 3C-SiC with Cr (1, 3, 5) % concentrations recorded at different temperatures (100K - 450K) using X-band rectangular cavity. The spectrum of pure 3C-SiC sample has shown the feature of resonance at resonance field $H_r = 329.05$ mT, corresponding to $g = 2.00$ which could be due to the defects present in the sample (V_{Si} , V_C) [12]. The line shape param-

eters and g value can be estimated from the analysis of the EPR spectra by fitting it to the two component Lorentzian function [13–15]. It comprises of two circular components of the exciting linearly polarized microwave magnetic field. It can be written as follows

$$\frac{dP}{dH} = \frac{2A}{\pi} \frac{d}{dH} \left(\frac{\Delta H}{4(H - H_0)^2 + \Delta H^2} + \frac{\Delta H}{4(H + H_0)^2 + \Delta H^2} \right) \quad (2)$$

where A represent area of the absorption curve, H_0 is the Resonance field and ΔH is the full width at half maximum in the absorption curve.

The pick width can be obtained from the fitting by using the formula $\Delta H_{pp} = \Delta H / \sqrt{3}$, and g value can be calculated from the fit parameter H_0 by resonance condition $g = h\nu / \mu_B H_0$, where h is Planck constant, ν is the microwave frequency and μ_B is the Bohr magneton. The variation of integrated intensity, Resonance field and peak to peak line width is shown in the Fig 4. Here the temperature dependence of line width can be explained by sum of both dipolar interaction and exchange narrowing mechanism in 3C-SiC. The ferromagnetic signature present in the sample can be attributed to the exchange interaction present in the system [16–19].

Even at very low doping concentration (1% Cr) in 3C-SiC, the EPR signal mainly shows very broad line. The reduction

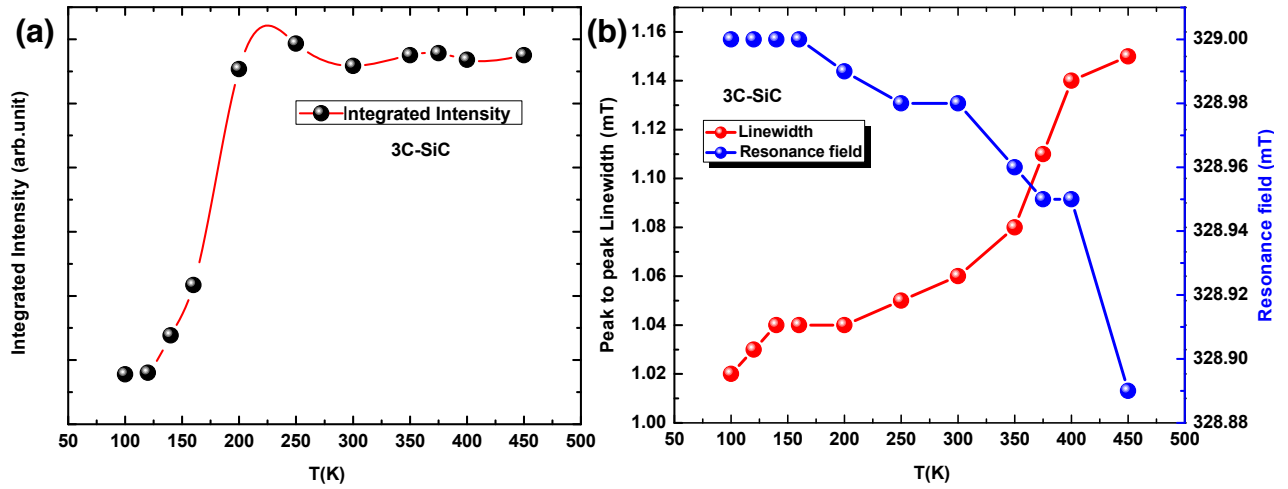


Figure 4. (a) Variation of Integrated Intensity with temperature of 3C-SiC (b) peak to peak line width and variation of resonance field with temperature for 3C-SiC.

in both line width and peak intensity has been observed with an increase in Cr^{3+} concentration. This broadening can be attributed to dipolar interaction between isolated Cr^{3+} ions at low concentration. The anti ferromagnetic coupling due to exchange interaction between Cr^{3+} nearby ions which is responsible for the reduction in intensity with an increase in Cr^{3+} concentration in host matrix has been observed in the EPR spectra both at 100 K as well as 300 K shown in Fig. 3(e, f). Signal-I is a sharp line corresponding to unresolved six hyperfine lines. However, the forbidden lines ($\Delta M_I = \pm 1$) present in the signal I are due to slight lattice distortion from an ideal tetrahedral structure. In Fig 3(b) is no forbidden transition is observed in the EPR spectra for $\text{Si}_{0.99}\text{Cr}_{0.01}\text{C}$, instead a small sharp line observed at 100K disappear with an increase in temperature. Another broad resonance is also obtained which increases in intensity with temperature. The spectrum of ($\text{Si}_{0.97}\text{Cr}_{0.03}\text{C}$) is shown in Fig. 3(c) also exhibits 3 different signals, such as

1. A dipolar interaction giving rise to a spectrum whose intensity increases and line width decreases with increase in temperature
2. A low field forbidden transition because of local distortion due to replacement of Cr^{3+} ion in place of Si^{4+}
3. A sharp line corresponding to Cr^{3+} ion available on the surface of the sample, whose intensity decreases with increase in temperature.

$\text{Si}_{0.95}\text{Cr}_{0.05}\text{C}$ EPR spectra shown in Fig. 3(d) indicates the dipolar interaction. It is possible that hyperfine average and demagnetization field is responsible for broad line observed in the sample. This dipolar broadening may be due to an interaction between nearest neighbor $\text{Cr}^{3+} - \text{Cr}^{3+}$ ions at higher concentration dopants in the host matrix. There is low field resonance for all the temperatures. This could be due to a

forbidden transition caused by a local distortion from regular tetrahedron by substitution of Cr^{3+} in place of Si^{4+} . With an increase in temperature from 100 K to 450 K, Signal (I) decreases in intensity and finally disappears. This is due to the presence of Cr^{3+} ions on the surface. Again, signal (II) intensity increases with increasing temperature and suddenly falls drastically at 300 K. This might be due to a phase transition (magnetic) in the system as is evident from Fig. 3(e, f). The g value for 1%, 3%, and 5% Cr doped 3C-SiC increases with an increase in composition due to an increase in dipolar interaction. But at 5% Cr substitution, more Cr^{3+} sits at the surface and dipole-dipole interaction intensity decreases as compared to the sharp line produced by Cr^{3+} ions. So the Cr^{3+} ion doping, affects the magnetic property by changing the structure of 3C-SiC with an increase in tetragonal phase of this compound and influences the Si/C vacancies defect formation process in the system. This is the reason for the formation and destruction of FM order in Cr doped 3C-SiC. There appears a ferromagnetic resonance (FMR) line due to Si/C vacancies (defects) in Cr doped samples along with Cr^{3+} lines. Further, there appears an intense and wide EPR line due to the interaction among the Cr^{3+} ions in the system on account of excess doping. The intensity and width of the line increases with increase in concentration [20, 21].

B. Q Band EPR Spectra of Cr Doped 3C-SiC

We have recorded the EPR spectra of 3C-SiC with chromium concentrations 1%, 3%, and 5% in Q-band (35.56 GHz) at different temperatures. The spectra are shown in Fig. 5(a, b, c, d,) where Cr^{3+} has d^3 electronic configuration with three unpaired electrons and normally is a quartet ($S = 3/2$) ground state. Depending on the symmetry of the Cr^{3+} site, and the distribution of charge compensating ‘holes’ around

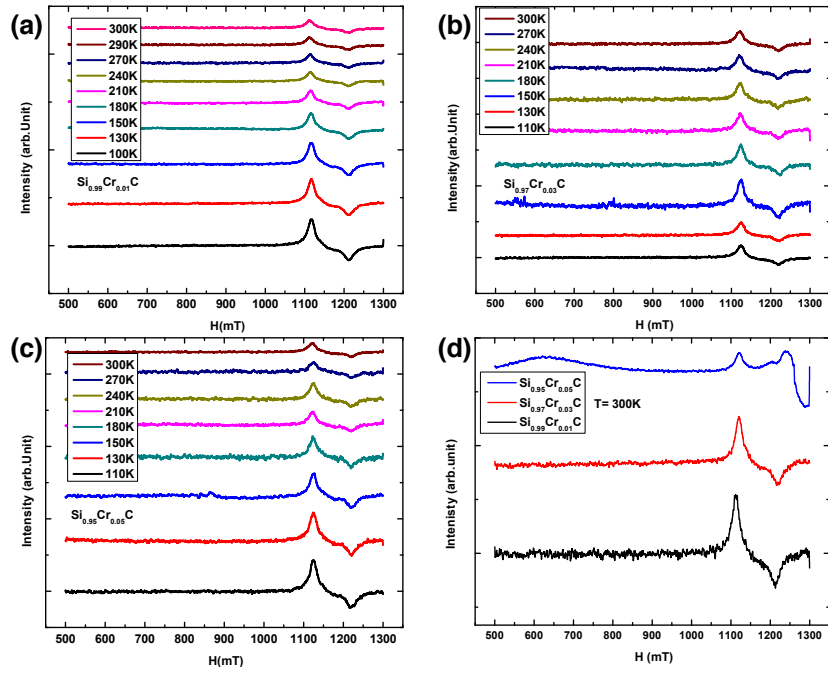


Figure 5. Q-band-EPR Spectra of undoped and Cr doped 3C-SiC. Fig. (a, b, c) represent the Cr^{3+} ion transition in Cr doped 3C-SiC. Fig. (d) represents all three transitions due to excess doping of Cr^{3+} for both low and high fields have been shown. Moreover, there is an additional peak which corresponds to the defect present in the system.

the defect, the zero-field spin-spin interactions between the electrons (even in the absence of the external field) lead to the presence of two Kramer's doublets with spin quantum numbers $|\pm 1/2\rangle$ and $|\pm 3/2\rangle$ with a separation of $2D$. Here D is the zero-field splitting when the symmetry of the crystal field is tetragonal. But due to charge compensating effect in a lattice, where Cr^{3+} is occupying Si^{4+} lattice sites or even in an interstitial site, the crystal field symmetry may well be rhombic leading to an E-term. The EPR spin Hamiltonian of Cr^{3+} can be written as

$$H = D \left[S_z^2 - \frac{1}{3} S(S+1) + \frac{E}{D} (S_x^2 - S_y^2) \right] + g_0 \beta S H, \quad (3)$$

where $D \rightarrow$ Zero field splitting parameter (ZFS), $E \rightarrow$ Rhombic splitting parameter at zero field, E/D is Rhombicity which is 0 (minimum) for an axial system and 0.5 (maximum) for a rhombic system. $g_0 \beta S H \rightarrow$ the paramagnetic contribution to the spin Hamiltonian arising from the isolated electrons.

For 3 unpaired electrons ($S = 3/2$): The four magnetic spin quantum numbers (sub levels) for m_s , can be written as $S_z = -3/2, -1/2, 1/2, \text{ and } 3/2$. So the energy for the $\pm 3/2$ level will be: $D[9/4 - 1/3(3/2 \times 5/2)] = D[9/4 - 5/4] = D$. And the energy for the $\pm 1/2$ level will be: $-D$. Energy level diagram of $S = 3/2$, Cr^{3+} progressively under crystal field, zero-field interaction and magnetic field is shown in Fig. 6. The separation between the two doublet levels is $2D$. Typical splitting of the spin energy levels in the case of $S = 3/2$ is given in the above figure. In the above figure, the three $M_s = \pm 1$ allowed transitions are indicated by the double-headed arrows. If the zero-field splitting is very large then $2D$ could be larger than the Micro Wave quantum.

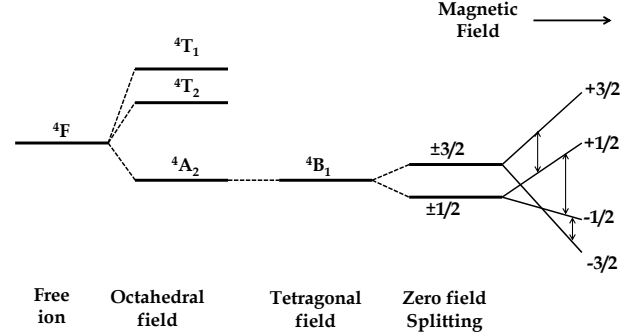


Figure 6. Energy Level Splitting in the presence of Magnetic Field

Only two of the allowed transitions, namely, $|-3/2\rangle \leftrightarrow |-1/2\rangle$ and $|-1/2\rangle \leftrightarrow |+1/2\rangle$ can be seen in the spectrum, and this is exactly the case in our Cr^{3+} doped 3C-SiC at X-band at Cr^{3+} concentrations of chromium namely 1%, and 3% [22, 23]. As the concentration of chromium is increased from 1% to 5%, there is a progressive anti-ferromagnetic exchange coupling between neighboring chromium ions leading to a reduction in the magnetization, and also narrowing of the spectral lines. At 5% concentration of chromium at Q-band frequencies we were able to see all the three zero-field transitions shown in Fig. 5(d).

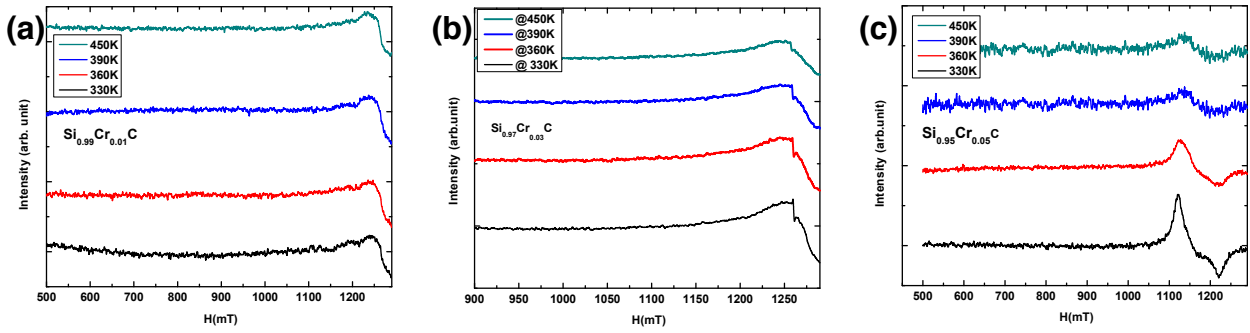


Figure 7. (a, b, c) Q-band EPR spectra variation with temperature for (1%, 3% & 5%) Cr doped 3C-SiC. It shows the Cr^{3+} transitions at higher temperature with different chromium concentration present in the system.

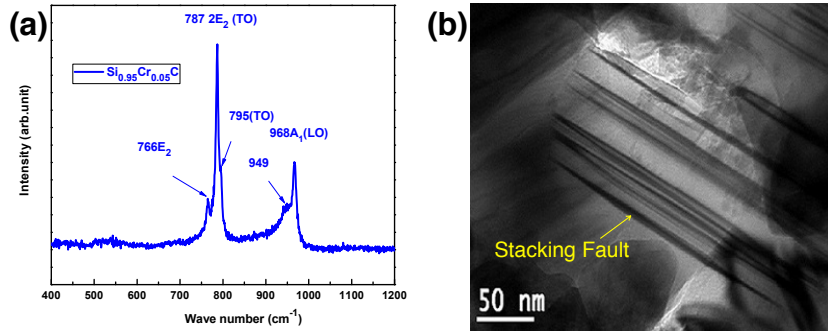


Figure 8. (a) Raman spectra of $\text{Si}_{0.95}\text{Cr}_{0.05}\text{C}$ and (b) HRTEM image of stacking faults. Dark lines represent stacking faults formed during the synthesis of the sample and corresponding peaks are shown in the Raman spectra.

In systems where the zero-field interaction is large, we treat each Kramer's doublet as a 'fictitious' spin 1/2 system, although the total spin remains 3/2. Under this circumstance, the g -values arising from these doublets will occur at g -factors which are far removed from $g = 2$. For transitions between $M_s = |\pm 3/2\rangle$, $|\pm 5/2\rangle$ and $|\pm 7/2\rangle$, Kramer's doublet will respectively occur at $g = 6$, 10 and 14. It is seen in the Q-band spectrum of 5% Cr^{3+} doped 3C-SiC that a broad absorption occurs at $g = 4$ corresponding to an allowed transition from $M_s = | +1/2\rangle \leftrightarrow | +3/2\rangle$ which was not accessible for the X-band quantum, but the Q-band quantum is adequate to cover this transition. Fig. 5(a) shows the room temperature Q band ESR spectra of 1%, 3% and 5% Cr doped 3C-SiC. At 5% Cr concentration level, we were able to see all the 3 transitions. The increase in Cr concentration enhances the formation of defects as confirmed by Raman and HRTEM studies. Moreover, as the temperature rises, the intensity of Q-Band EPR spectra decreases with an increase in concentration. This might be due to the fact that an increase in Cr concentration favors to build up the anti-ferromagnetic interactions in the system. This is also evident from the magnetic measurement data. The magnetic moment suffers a reduction as the Cr concentration increases in the system. There is yet another possibility in the case of Cr^{3+} concentration exceeding 3%.

With an increase in the hole concentration due to charge compensation, it is possible that excess chromium may act as a hole-trap, generating a small amount of Cr^{4+} which will

get stabilized because of its charge equivalence to the lattice Si^{4+} substitution site, further favored by its reduction in ionic radius. If this is in fact what happens upon excess doping of Cr^{3+} , then we have a small percentage of d^2 in Cr^{4+} which is a triplet state and is known to have a very large zero-field splitting as observed by Baranov et. al. [24]. These authors report resonances with $g = 3.7$ and 1.77 for Cr^{4+} in chromium doped 6H-SiC. It can be seen in our Q-band spectra that at high Cr concentration, there is a reduction in Cr^{3+} features and simultaneous appearance of new features at $g = 3.8$ and 1.8 . This presumably is due to the formation of Cr^{4+} by hole trapping on excess Cr^{3+} . In addition to this, Q-band EPR spectra at high temperature (330-450)K confirms the Cr valence state as Cr^{3+} and magnetic phase transition in Cr doped 3C-SiC, as shown in Fig. 7(a, b, c).

IV. RAMAN STUDY

Raman scattering spectra of 3C-SiC and Cr doped 3C-SiC with different doping concentrations (1, 3, 5) % were measured from 100 K to 840 K, see Fig. 1(b). It can be seen that there are two characteristics overlapping bands at 796 cm^{-1} and 789 cm^{-1} observed in the 3C-SiC system along with some additional defect peaks [25, 26]. These are assigned to the folded transverse optical (FTO) bands, folded longitudinal

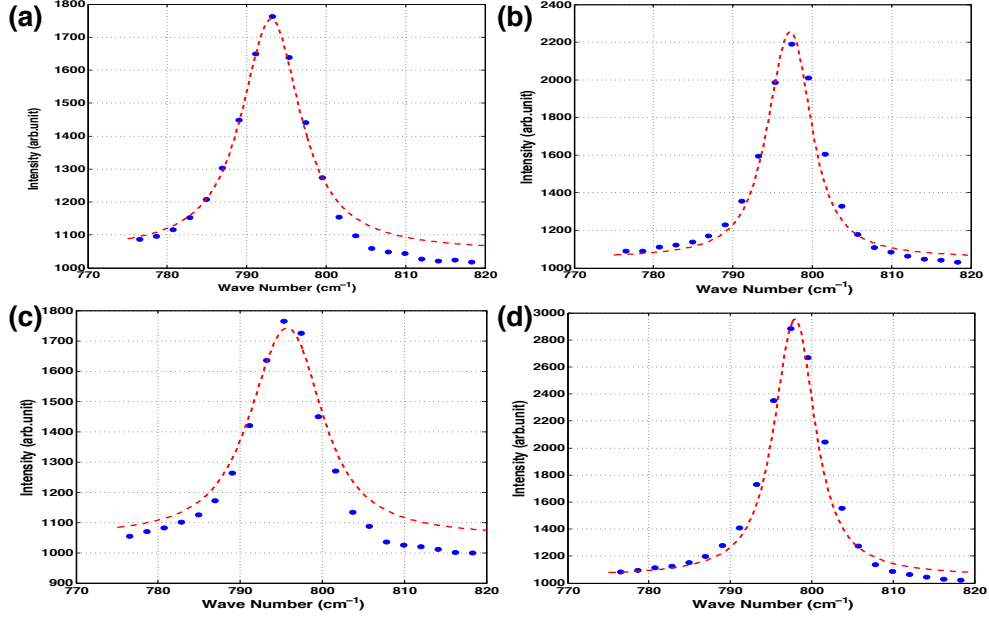


Figure 9. (a, b, c, d) TO Fit for undoped and Cr doped 3C-SiC at 100K. In all four cases blue circles represent the experimental data while dotted lines represent the fit.

Sample	3C-SiC	Si _{0.99} Cr _{0.01} C	Si _{0.97} Cr _{0.03} C	Si _{0.95} Cr _{0.05} C
A (cm ⁻¹)	795.1	795.2	795.0	800.0
B (cm ⁻¹)	15.0	32.5	15.0	23.7
L(Å)	25.5	37.7	30.0	25.5
Γ ₀ (cm ⁻¹)	11.7	8.5	11.7	8.5

Table I. Fitted parameters on TO modes for samples, excited by the 488 nm at T=100K.

optical (FLO) bands, and defect peaks respectively. However TO band is doubly degenerate. But due to the reduction of symmetry in the system from cubic to other crystal structure on account of the formation of other polytypes or defects (stacking faults), the degeneracy is lifted and transverse component shifts to lower wave number side. The increase in defect number density broadens the observed signals and in the case of excess number density it may induce stacking disorder in the system. Furthermore, signature can be seen in the spectra as an additional peak at lower wave number as shown in Fig. 8. As a result of this, unit cell volume of 3C-SiC polytype increases, and the Brillouin zone is reduced by zone folding phenomena. This results in the appearance of new phonon modes (i.e. folded modes) in the spectra [26]. A similar effect can also be realized in a system where the periodicity has been lost due to disorder or defects present in it. This allows the Raman scattering with wave vector $\mathbf{k} = \mathbf{0}$ to appear in the spectrum due to the relaxation in wave vector selection rule. The band at 789 cm⁻¹ is a FTO band caused by an effective reduction in symmetry. A separation of 7 cm⁻¹, has been found between TO and FTO bands, similar to that found in 6H-SiC [27]. Similar to the peak at (767 cm⁻¹), FTO band of the 6H structure, another shoulder peak at 766 cm⁻¹ has been

identified as a signature of random stacking fault present in the system. The Eq. 4 used for the fitting of experimental data by using the spatial correlation model (SCM) is given below:

$$I(\omega) \propto \int_0^1 \exp\left(\frac{-q^2 L^2}{4}\right) \frac{d^3 q}{[\omega - \omega(q)]^2 + [\Gamma_0/2]^2}, \quad (4)$$

here $I(\omega) \rightarrow$ Transverse Optical Raman scattering intensity, $q \rightarrow$ function of $2\pi/a$, $a \rightarrow$ Lattice constant, $L \rightarrow$ Phonon propagation length characterizing the quality of the crystals, $\Gamma_0 \rightarrow$ FWHM of the Raman peak of TO (LO) phonon of the bulk crystalline 3C-SiC. Fitting of experimental Raman data with theoretically stimulated spectra for 100K and 800K data are shown respectively in Figs. 9 and 10. The corresponding fitting parameters are shown in Tables I and II. From the analysis of the TO mode recorded at RT, reduced crystallinity and formation of stacking faults were observed due to excess doping of Cr³⁺ ions [26]. In addition to this, the possibility of the formation of Longitudinal optical plasmon mode in polar semiconductor is also more likely. Since SiC is a polar semiconductor, the asymmetric broadening of FLO mode in Cr doped 3C-SiC can be attributed to the Longitudinal Optic-

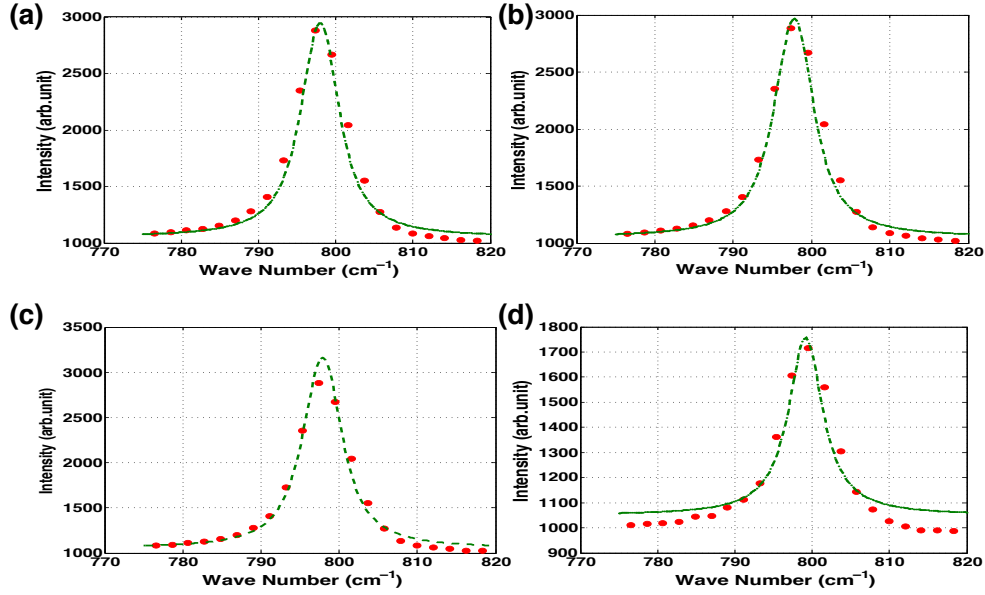


Figure 10. (a, b, c, d) TO fit of Raman spectra of undoped and Cr doped 3C-SiC at 800K. In all four cases red circles represent the experimental data whereas dotted lines represent the fit.

Sample	3C-SiC	Si _{0.99} Cr _{0.01} C	Si _{0.97} Cr _{0.03} C	Si _{0.95} Cr _{0.05} C
A (cm ⁻¹)	795.0	796.0	795.0	800.0
B (cm ⁻¹)	15.0	23.7	21.2	41.2
L(Å)	25.4	35.5	20.5	20.7
Γ ₀ (cm ⁻¹)	11.7	5.3	8.5	11.6

Table II. Fitted parameters on TO modes for samples, excited by the 488 nm at T = 800K.

al Plasmon Coupling mode (LOPC) present in the system. In order to check the validity of the assumption, we tried to fit the experimentally obtained data to LOPC model. It fits quite well as can be seen in Figs. 11 and 12. Corresponding fitting parameters can be found in Tables III and IV. The LOPC fitting was done with the experimental data in a temperature range (110 – 840) K. There is a linear relationship between carrier concentration and Raman shift of the LOPC mode in SiC. The non monotonous variation of LOPC peak with temperature and carrier concentration can be explained as a cou-

pling between the temperature dependent LOPC mode with carrier concentration [28–30]. The variation of peak intensity and peak position with temperature and doping concentration was analyzed by Line shape fitting, using Eq. 5 and classical dielectric function (CDF) for all Cr doped 3C-SiC samples.

$$I_{\text{LOPC}} = \frac{d^2\mathbf{S}}{d\omega d\Omega} \Big|_A = \frac{16\pi h n_2}{V_0^2 n_1} \frac{\omega_2^4}{C^4} \left(\frac{d\alpha}{dE} \right) (\epsilon_\infty + 1) A \text{Im} \left(-\frac{1}{\epsilon} \right) \quad (5)$$

where A and Δ are respectively defined by Eqs. 6 and 7

$$A = 1 + 2C \frac{\omega_T^2}{\Delta} \left[\omega_p^2 \gamma (\omega_T^2 - \omega^2) - \omega^2 \eta (\omega^2 + \gamma^2 - \omega_p^2) \right] + \frac{C^2 \omega_T^4}{\Delta (\omega_L^2 - \omega_T^2)} \left[\omega_p^2 \gamma (\omega_L^2 - \omega_T^2) + \omega_p^2 \eta (\omega_p^2 - 2\omega^2) + \omega^2 \eta (\omega^2 + \gamma^2) \right] \quad (6)$$

$$\Delta = \omega_p^2 \gamma \left[(\omega_T^2 - \omega^2)^2 + (\omega \eta)^2 \right] + \omega^2 \eta (\omega_L^2 - \omega_T^2) (\omega^2 + \gamma^2) \quad (7)$$

In these equations, $\omega_L \rightarrow$ LO mode frequency, $\omega_T \rightarrow$ TO

mode frequency, $\eta \rightarrow$ phonon damping constant, $\gamma \rightarrow$ plasma damping constant, $\alpha \rightarrow$ Polarizability, $E \rightarrow$ Electric field, n_2 is the refractive index and ω_2 is the scattered frequency.

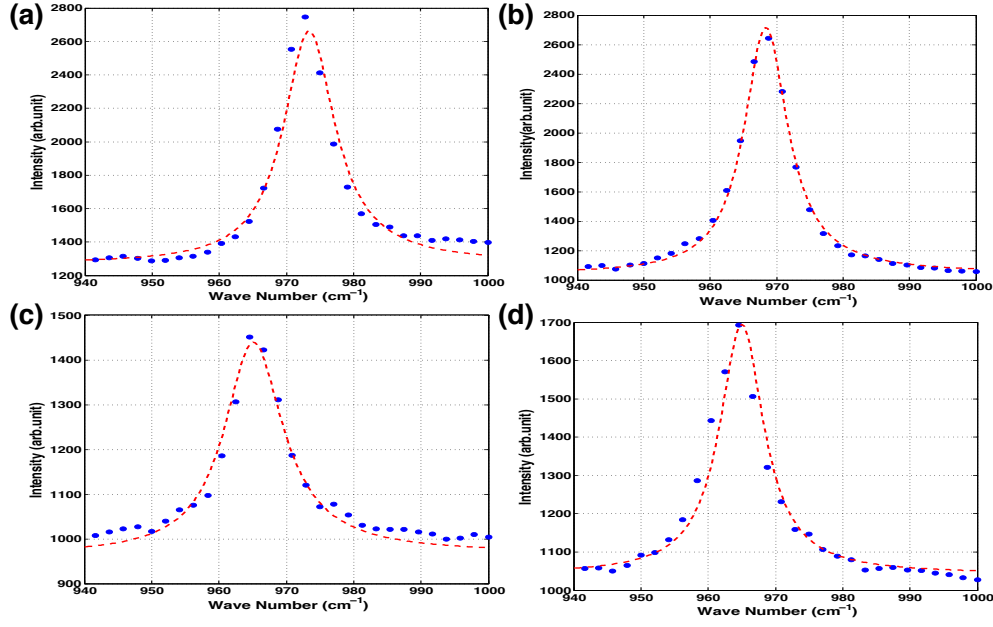


Figure 11. (a, b, c, d) LOPC fit of Raman spectra of undoped and Cr doped 3C-SiC at 100 K. In all four cases blue circles represent the experimental data while dotted lines represent the fit.

Sample	3C-SiC	Si _{0.99} Cr _{0.01} C	Si _{0.97} Cr _{0.03} C	Si _{0.95} Cr _{0.05} C
ω_p (cm ⁻¹)	5.0	48.9	92.7	136.6
γ (cm ⁻¹)	89.4	234.4	136.5	92.78
η (Å)	1.0	2.2	1.1	1.2
n ($\times 10^{16}$ cm ⁻³)	0.1	11.4	41.0	89.1

Table III. Fitted parameters on LO- phonon modes for samples, excited by the 488 nm at T=100K.

The total Dielectric function due to phonons and plasmons can be described as

$$\epsilon(\omega) = \epsilon_{\infty} \left(\frac{1 + \omega_L^2 - \omega_T^2}{\omega_T^2 - \omega^2 - i\omega\eta} - \frac{\omega_p^2}{\omega(\omega + i\eta)} \right), \quad (8)$$

$$\omega_p^2 = \frac{4\pi n e^2}{\epsilon_{\infty} m^*}, \quad (9)$$

where $C \rightarrow$ Faust-Henry coefficient = 0.35. It can also be modified by Cr doping in pure 3C-SiC because of deformed potential present in the system

$$C = C_{FH} \left\{ \frac{\epsilon(r)_{\infty} \omega_T^2 \left[\omega(r)_{Lm}^2 - \omega(r)_{Tm}^2 \right]}{f_{\infty} \omega_{Tm}^2 (\omega_L^2 - \omega_T^2)} \right\}^{1/2}, \quad (10)$$

here $\omega_p \rightarrow$ Plasma frequency, $n \rightarrow$ free carrier concentration, $m^* \rightarrow$ effective mass and $\epsilon_{\infty} \rightarrow$ High field dielectric constant, $\omega_{Tm} \rightarrow$ Transverse Optical mode frequency, $\omega_{Lm} \rightarrow$ Longitudinal Optical mode frequency. Raman scattering intensity of

LO mode can also be described by a Lorentz profile function for undoped 3C-SiC which can be expressed as

$$I_{A_1(LO)} = \frac{I_0}{\left(\frac{\omega - \omega_s}{\Gamma_s} \right)^2 + 1}, \quad (11)$$

where $\omega_s \rightarrow$ LO phonon frequency near the Brillouin zone center, $\Gamma_s \rightarrow$ Line width of peak and $I_0 \rightarrow$ constant.

The LOPC frequency can be calculated by using the equation

$$\omega_{LOPC}^2 = \frac{(\omega_p^2 + \omega_{LO}^2) + \sqrt{(\omega_p^2 + \omega_{LO}^2)^2 - 4\omega_p^2 \omega_{TO}^2}}{2}. \quad (12)$$

The carrier density calculated by using LOPC fit with experimental data varies from 1.8×10^{15} to 4.2×10^{17} cm⁻³ with temperature. The damping of phonon and plasmon could be the reason for this behavior in the Raman spectra of Cr doped 3C-SiC. Phonon life times were calculated using Raman FWHM through the energy-time uncertainty relation, where ΔE is the Raman FWHM in units of cm⁻¹ and Planck

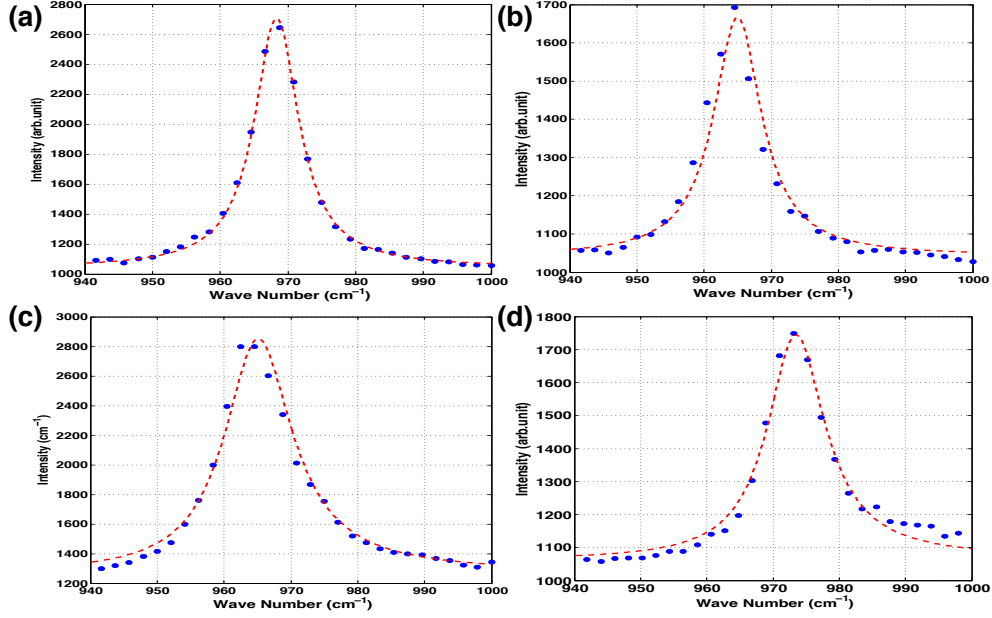


Figure 12. (a, b, c, d) LOPC fit of undoped and Cr doped 3C-SiC at 800K. In all four cases blue circles represent the experimental data while dotted lines represent the fit.

Sample	3C-SiC	Si _{0.99} Cr _{0.01} C	Si _{0.97} Cr _{0.03} C	Si _{0.95} Cr _{0.05} C
ω_p (cm ⁻¹)	36.6	180.5	201.6	312.2
γ (cm ⁻¹)	90.0	136.1	168.8	224.4
η (Å)	1.0	1.2	1.1	1.1
n ($\times 10^{16}$ cm ⁻³)	6.4	155.6	194.0	465.5

Table IV. Fitted parameters on LO- phonon modes for samples, excited by the 488 nm at T = 800K.

constant $h = 5.3 \times 10^{-12}$ cm⁻¹s. The phonon lifetime τ is largely affected by the reduction of the symmetry present in the system and can be explained by two mechanisms called (a) phonon-carrier scattering and (b) phonon-phonon scattering respectively. The life time calculated from Raman spectra lies in the range of picosecond which indicates that the carrier - phonon interaction scattering is the dominant mechanism [31].

V. ISOTHERMAL MAGNETIZATION STUDY

DC magnetic measurements were carried out using vibrating sample magnetometer in the low and high temperature regimes. Fig. 13 shows the FC (field cool) – ZFC (zero field cool) plot of undoped and Cr doped 3C-SiC up to 300K. In the case of pure 3C-SiC, FC-ZFC curves show a small bifurcation. This might be due to the defects present in the sample. But the magnitude of magnetization is extremely small. The isothermal field variation shows small hysteresis with low moment at 5K, whereas only a diamagnetic response is observed above 80K. The weak ferromagnetic like response at 5K may

be due to the defects (Si or C vacancies) present in the sample. The electron trapped in such vacant sites (F-Centers) may interact to give a weak ferromagnetic response. The Cr doped samples show a clear bifurcation up to room temperature. The clear bifurcation of FC-ZFC plot of Cr doped sample indicates the ferromagnetic order present in the system. The Curie temperature (T_C) is found to be above 780 K as shown in the Fig. 13 and the transition becomes less sharper with an increase in Cr Concentration [32]. The Corresponding M-H curve is shown in Fig. 14(a, b, c). It can be seen that hysteresis goes on decreasing with an increase in temperature. With increasing Cr concentration, though hysteresis increases, the saturation magnetization decreases. This may be due to setting up of anti ferromagnetic order in the system which happens further on account of excess doping of Cr. This is also evident from the high temperature M-T plots of all the doped samples. The origin of long range ferromagnetic order in Cr, Mn, Fe, Co and Ni doped wide band gap semiconductors have been a topic of research for decades. As physical properties of materials are intrinsically related to the structure of the materials, the synthesis procedure, experimental conditions and morphology plays very decisive role. We have prepared the Cr doped 3C-SiC by carbothermal reduction of silica from rice

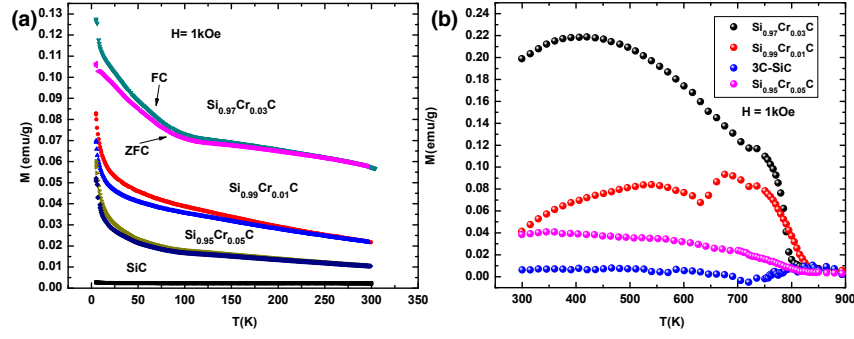


Figure 13. (a) FC-ZFC Plots of undoped and Cr doped 3C-SiC. The concave upward nature of both FC-ZFC plots with field indicates the ferromagnetic nature of the samples. (b) M-T Plots of undoped and Cr doped 3C-SiC samples. It can be seen that the transition is sharper with increasing Cr concentration (1%, 3%) and becomes broader at 5% Cr concentration due to the present of anti ferromagnetic interaction present in the system.

husk at extremely high temperature (1500°C). The experimental conditions is very much liable for the formation of the lattice defects such as vacancies and interstitial in the system. The substitution of Cr at the Si site turns out to be more preferable under these experimental condition. This has been confirmed by structural and spectroscopic investigation via XRD, Raman and EPR techniques. Moreover, the Cr substitution at Si sites exhibits more stable ferromagnetism [8]. From EPR, it is confirmed that the Cr ion is present at both tetrahedral and octahedral co-ordination sites and is in the trivalent state. The chromium in Cr^{3+} state can exhibit low spin or high spin state. Usually Cr^{3+} in low spin state does not induce magnetism but in high spin state can induce a weak magnetization in the system. The long range order in magnetic interaction can be explained by the exchange interaction between F-Centers (an electron trapped with positive charge vacancy) in the system. This is known as the so called Bound Magnetic Polaron Model and was first invoked to explain the magnetic interaction in Oxide based Dilute magnetic semiconductors [33–35]. Here, the [Si, C] vacancy, being positively charged, traps the electron and it is referred to as an F center. Si/C vacancies in this system are adjacent to the Cr dopants in the lattice, leading to an F-center exchange. In order to explain the mechanism responsible for magnetic interaction in the system, the role of magnetic impurity (Carrier concentration) and vacancy density has to be taken into consideration. In Cr doped 3C-SiC, the interaction between vacancies (Si/C) nearer to Cr dopants leads to a ferromagnetic order in the system. It is possible that the doping of 1% and 3% Cr in the host matrix might have increased the (Si/C) vacancies with the regular substitution at Si sites that resulted in increased magnetization of the system. Further increase in Cr concentration might have exceeded the solubility limit. Due to this increase, there is a net reduction in the magnetization in 5% Cr doped 3C-SiC. Due to excess carrier concentration, the distance between Cr–Cr ions decreases and Cr also goes to an interstitial position in the lattice. This occupancy destroys the F-centers exchange interaction inducing anti ferromagnetic interaction the system. The net result is reduction in total magnetization. This can be confirmed from the sharp line in EPR spectra shown in Fig. 3(b, c, d).

Thus, along with Cr dopants' density, the F-centers, i.e., the Si vacancies play a crucial role in invoking a ferromagnetic exchange interaction through carrier mediated Polaron interaction. To check the validity of the BMP model, we have fitted the experimental magnetization data to the relation

$$M = M_0 L(x) + \chi_m H \quad (13)$$

$$M_0 = Nm_s, L(x) = \coth(x) - \frac{1}{x}, X = \frac{m_{\text{eff}} H}{k_B T} \quad (14)$$

where

$ML_0(x) \rightarrow$ BMP contribution

$\chi_m H \rightarrow$ Paramagnetic contribution

$M_0 = Nm_s$

$N \rightarrow$ No of BMP involved in the interaction.

$m_s \rightarrow$ Effective spontaneous moments per BMP

$L(x) \rightarrow$ Langevin function

$X \rightarrow$ True spontaneous moment per BMP and

at higher temperature $m_s = m_{\text{eff}} M_0$,

$m_s, m_{\text{eff}} \rightarrow$ Variable in fitting process

$m_{\text{eff}} \rightarrow$ The spontaneous moment per BMP = 10^{-17}

Details of the fitting parameters have been given in Table V. We propose the BMP model to explain the high temperature behavior of Cr doped 3C-SiC. To build up a long range BMP percolation in the system, the concentration of BMP has to be $10^{20}/\text{cm}^3$. However, the number density obtained from the fit is smaller than this number. The fitting of experimental magnetization data to the theoretical BMP model is shown in the Fig. 15(a, b, c). The calculated low concentration of BMPs can't be held responsible for the observed magnetic interaction in Cr doped 3C-SiC. The effective Bound Magnetic Polaron radius is found to be $\simeq 17$ nm. The long range magnetic order in the system can be established due to BMP percolation in the presence of the lattice defect in the system. In addition to that, the role of Magnetic impurity is also significant. If there is more BMP density, the possibility of the interaction between two isolated Cr ions will be less, otherwise there will be isolated Cr-Cr ions which can have rare FM interaction

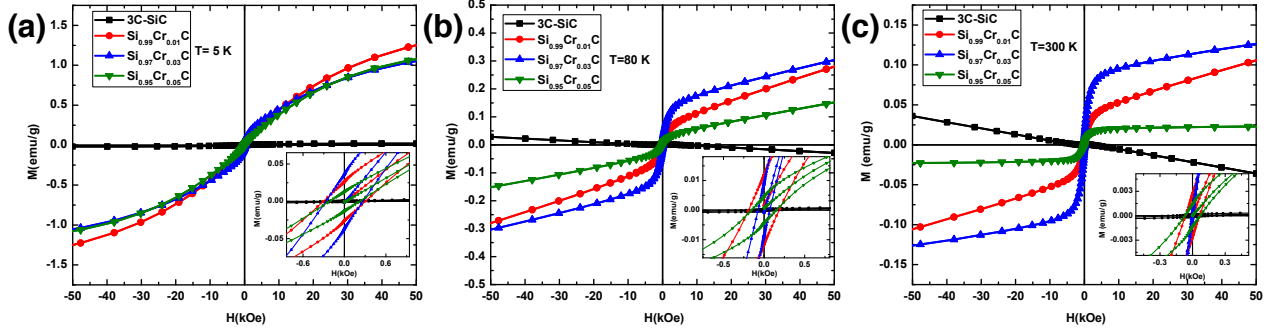


Figure 14. (a, b, c) M-H plots of undoped and Cr doped 3C-SiC at 5K, 80K and 350K respectively. Pure 3C-SiC shows clear diamagnetic behavior with increase in temperature. On the other hand, coercivity of Cr doped samples decreases with increase in temperature.

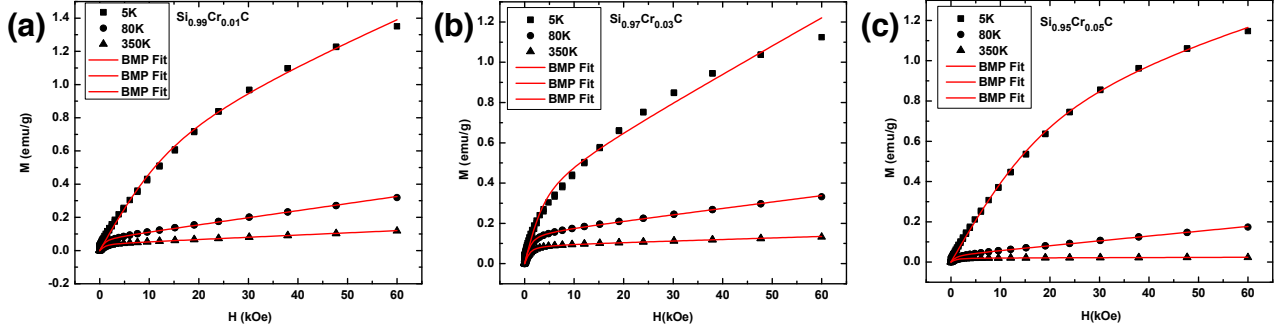


Figure 15. BMP fit with experimental data of Cr doped 3C-SiC.

without the presence of defects [36, 37]. This is because, in case of short range interaction, it would align in an anti-ferromagnetic manner. So the doped magnetic cation prevents it from happening and helps to set a long range magnetic interaction in the system. The blue shift of the Raman spectra clearly reveals the formation of Si/C vacancies. The no of cation sites V_C within a sphere of radius r_H ranges from 10 to 100 depending upon the value of r_H . The lower value of measured magnetization in undoped 3C-SiC (10^{-3} emu/g) must have been due to defect induced origin as has been mention in the literature. But with Cr^{3+} ion doping, magnetization value has increased in Cr doped 3C-SiC. Thus it seems that both magnetic ions as well as defects are important elements to attain high moment as well as high T_C as observed here in our sample. Fig 16(a, b) shows ferromagnetic part contributed from BMP percolation after subtracting the paramagnetic part [38]. Magnetic moment of 3% Cr doped sample is high as compared to 5% Cr doped sample. A plausible reason can be an increase in Cr concentration, as it favors the formation of more no of defects and hence more no of BMPs. But further increase in Cr concentration (5%) may favour the initiative of exchange interaction and reduce the magnetization as the distance between Cr-Cr ions decreases.

VI. CONCLUSION

In this study, for the first time, we have reported room temperature ferromagnetism in Cr doped 3C-SiC and found a noble method to determine the charge carrier density by using the LOPC model. The X-band EPR spectra of Cr doped 3C-SiC reveals multi valence states of chromium. The Q-band EPR spectra clearly reveals the presence of Cr^{3+} ions in the system. The non monotonous variation of Raman shift and phonon life time can be explained by invoking phonon - carrier scattering process (LOPC model). Room Temperature FM has been observed in Cr doped 3C-SiC. The observed FM could be explained on the basis of intrinsic exchange interaction of Cr ions and V_{Si} , V_C defects present in the system. Both Cr^{3+} ions, as well as defects, play a decisive role to attain a high temperature long range magnetic order. Substitution of Cr^{3+} in place of Si^{4+} enhances the defect concentration and thereby sets up long range magnetic order in the system. But the excess doping of Cr ion in the host matrix introduces anti-ferromagnetic order and leads to the suppression of the ferromagnetic interaction caused by BMP percolation. Solubility limit of Cr in 3C-SiC has been found to be 3%.

ACKNOWLEDGMENTS

One of the authors, Gyanti Prakash Moharana, thanks IIT Madras for the financial support. Rahul Kothari sincerely acknowledges the Institute Post Doctoral Fellowship of IIT Ma-

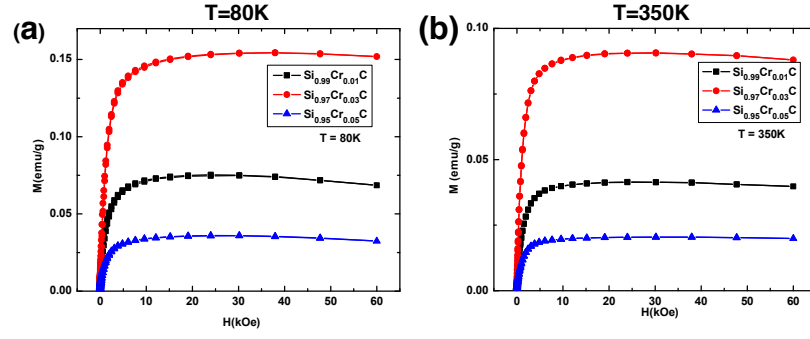


Figure 16. BMP fit with experimental data after subtracting para magnetic contribution showing ferromagnetic part of Cr doped 3C-SiC.

T(K)	$M_{\text{eff}} \times 10^{-17}$ (emu)	$\chi_m \times 10^{-6}$ (emu/gOe)	$N \times 10^{17}$ (cm $^{-3}$)	M_s (emu /g)	H_C (Oe)	M_r (m emu/g)
350	7.65	1.30	0.016	0.04	64	0.002
80	1.79	4.17	0.013	0.07	180	0.011
5	104	0.11	236	0.77	300	0.023

(a) BMP Fitting Parameters of $\text{Si}_{0.99}\text{Cr}_{0.01}\text{C}$

T(K)	$M_{\text{eff}} \times 10^{-17}$ (emu)	$\chi_m \times 10^{-6}$ (emu/gOe)	$N \times 10^{17}$ (cm $^{-3}$)	M_s (emu /g)	H_C (Oe)	M_r (m emu/g)
350	8.7	70.02	0.033	0.09	8	0.006
80	1.92	3.09	0.025	0.15	71	0.009
5	328	0.12	43.320	0.44	268	0.036

(b) BMP Fitting Parameters of $\text{Si}_{0.97}\text{Cr}_{0.03}\text{C}$

T(K)	$M_{\text{eff}} \times 10^{-17}$ (emu)	$\chi_m \times 10^{-6}$ (emu/gOe)	$N \times 10^{17}$ (cm $^{-3}$)	M_s (emu /g)	H_C (Oe)	M_r (m emu/g)
350	8.15	536	0.008	0.02	70	0.001
80	1.78	2.35	0.065	0.03	150	0.004
5	780	5.85	390.210	0.94	210	0.013

(c) BMP Fitting Parameters of $\text{Si}_{0.95}\text{Cr}_{0.05}\text{C}$

Table V. BMPs Fitting parameters extracted from experimental data by using BMP model.

dras. We greatly acknowledge DST-SAIF, IIT Madras for VSM and EPR measurements. We thank Prof. Sankaran Sub-

ramanian (Adjunct Professor & INSA Senior Scientist, Department of Chemistry and Sophisticated Analytical Instrument Facility) for useful discussion on the EPR data analysis.

- [1] T. Dietl, H. Ohno, F. Matsukura, J. Cibert, and D. Ferrand. Zener Model Description of Ferromagnetism in Zinc-Blende Magnetic Semiconductors. *Science*, **287**(5455):1019–1022, 2000.
- [2] M. L. Reed, N. A. El-Masry, H. H. Stadelmaier, M. K. Ritums, M. J. Reed, C. A. Parker, J. C. Roberts, and S. M. Bedair. Room temperature ferromagnetic properties of (Ga, Mn)N. *Applied Physics Letters*, **79**(21):3473–3475, 2001.
- [3] H. Saadaoui, X. Luo, Z. Salman, X. Y. Cui, N. N. Bao, P. Bao, R. K. Zheng, L. T. Tseng, Y. H. Du, T. Prokscha, A. Suter, T. Liu, Y. R. Wang, S. Li, J. Ding, S. P. Ringer, E. Morenzoni, and J. B. Yi. Intrinsic Ferromagnetism in the Diluted Magnetic Semiconductor Co : TiO_2 . *Phys. Rev. Lett.*, **117**:227202, Nov 2016.
- [4] S. K. Singh, B. C. Mohanty, and S. Basu. Synthesis of SiC from rice husk in a plasma reactor. *Bulletin of Materials Science*, **25**(6):561–563, Nov 2002.
- [5] G. Mishra, S. Mohapatra, S. Prusty, M. K. Sharma, R. Chatterjee, S. K. Singh, and D. K. Mishra. Magnetic properties of nanocrystalline β -SiC. *J. Nanosci. Nanotechnology*, **11**:5049–53, 2011.
- [6] C G Jin, X M Wu, L J Zhuge, Z D Sha, and B Hong. Electric and magnetic properties of Cr-doped SiC films grown by dual ion beam sputtering deposition. *Journal of Physics D: Applied Physics*, **41**(3):035005, 2008.
- [7] Zhao Huang and Qianwang Chen. Magnetic properties of Cr-doped 6H-SiC single crystals. *Journal of Magnetism and Magnetic Materials*, **313**(1):111 – 114, 2007.

- [8] Yoon-Suk Kim and Yong-Chae Chung. Magnetic and Half-Metallic Properties of Cr doped β -SiC. *IEEE Transaction on Magnetics*, **41**:2733–2735, 2005.
- [9] A. Los and V. Los. Magnetic states of transition metal impurities in silicon carbide. *J. Phys: Condens. Matter*, textbf21:206004–11, 2009.
- [10] K. Bouziane, M. Mamor, M. Elzain, Ph. Djemia, and S. M. Chérif. Defects and magnetic properties in Mn-implanted 3C-SiC epilayer on Si(100): Experiments and first-principles calculations. *Phys. Rev. B*, **78**:195305, Nov 2008.
- [11] N. T. Son, P. Carlsson, J. ul Hassan, E. Janzén, T. Umeda, J. Isoya, A. Gali, M. Bockstedte, N. Morishita, T. Ohshima, and H. Itoh. Divacancy in 4H-SiC. *Phys. Rev. Lett.*, **96**:055501, Feb 2006.
- [12] Yu Liu, Gang Wang, Shunchong Wang, Jianhui Yang, Liang Chen, Xiubo Qin, Bo Song, Baoyi Wang, and Xiaolong Chen. Defect-Induced Magnetism in Neutron Irradiated 6H-SiC Single Crystals. *Phys. Rev. Lett.*, **106**:087205, Feb 2011.
- [13] J. Yang, X. Rong, D. Suter, and Y. P. Sun. Electron paramagnetic resonance investigation of the electron-doped manganese $\text{La}_{1-x}\text{Te}_x\text{MnO}_3$ ($0.1 \leq x \leq 0.2$). *Phys. Chem. Chem. Phys.*, **13**:16343–16348, 2011.
- [14] Janhavi P Joshi, K Vijaya Sarathy, A K Sood, S V Bhat, and C N R Rao. An electron paramagnetic resonance study of electron-hole asymmetry in charge ordered $\text{Pr}_{1-x}\text{Ca}_x\text{MnO}_3$ ($x = 0.64, 0.36$). *Journal of Physics: Condensed Matter*, **16**(16):2869, 2004.
- [15] V. A. Ivanshin, J. Deisenhofer, H.-A. Krug von Nidda, A. Loidl, A. A. Mukhin, A. M. Balbashov, and M. V. Eremin. ESR study in lightly doped $\text{La}_{1-x}\text{Sr}_x\text{MnO}_3$. *Phys. Rev. B*, **61**:6213–6219, Mar 2000.
- [16] Bo Peng, Yuming Zhang, Yutian Wang, Hui Guo, Lei Yuan, and Renxu Jia. Ferromagnetism observed in silicon-carbide-derived carbon. *Phys. Rev. B*, **97**:054401, Feb 2018.
- [17] A. Zorko, M. Pregelj, H. Luetkens, A.-K. Axelsson, and M. Valant. Intrinsic paramagnetism and aggregation of manganese dopants in SrTiO_3 . *Phys. Rev. B*, **89**:094418, Mar 2014.
- [18] A. Zorko, M. Pregelj, M. Gomilšek, Z. Jagličić, D. Pajić, M. Telling, I. Arčon, I. Mikulska, and M. Valant. Strain-Induced Extrinsic High-Temperature Ferromagnetism in the Fe-Doped Hexagonal Barium Titanate. *Scientific Reports*, **5**:7703 EP, 01 2015.
- [19] S. Zimmermann, F. Steckel, C. Hess, H. W. Ji, Y. S. Hor, R. J. Cava, B. Büchner, and V. Kataev. Spin dynamics and magnetic interactions of Mn dopants in the topological insulator Bi_2Te_3 . *Phys. Rev. B*, **94**:125205, Sep 2016.
- [20] Sushil K. Misra, S. I. Andronenko, S. Rao, Subray V. Bhat, Chadd Van Komen, and A. Punnoose. Cr³⁺ electron paramagnetic resonance study of $\text{Sn}_{1-x}\text{Cr}_x\text{O}_2$ ($0.00 \leq x \leq 0.10$). *Journal of Applied Physics*, **105**(7):07C514, 2009.
- [21] Kusuma URS, S. V. Bhat, and Vinayak Kamble. On exceeding the solubility limit of Cr^{+3} dopants in SnO_2 nanoparticles based dilute magnetic semiconductors. *Journal of Applied Physics*, **123**(16):161518, 2018.
- [22] A. M. Ferretti, A.-L. Barra, L. Forni, C. Oliva, A. Schweiger, and A. Ponti. Electron Paramagnetic Resonance Spectroscopy of Iron(III)-Doped MFI Zeolite. 1. Multifrequency CW-EPR. *The Journal of Physical Chemistry B*, **108**(6):1999–2005, 2004.
- [23] J.A. Weil, J.R. Bolton, and J.E. Wertz. *Electron Paramagnetic Resonance: Elementary Theory and Practical Applications*. Wiley, 1994.
- [24] P G Baranov, V A Khramtsov, and E N Mokhov. Chromium in silicon carbide: electron paramagnetic resonance studies. *Semiconductor Science and Technology*, **9**(7):1340, 1994.
- [25] H. Yugami, S. Nakashima, A. Mitsuishi, A. Uemoto, M. Shigetani, K. Furukawa, A. Suzuki, and S. Nakajima. Characterization of the free-carrier concentrations in doped β SiC crystals by Raman scattering. *Journal of Applied Physics*, **61**(1):354–358, 1987.
- [26] Stefan Rohmfeld, Martin Hundhausen, and Lothar Ley. Raman scattering in polycrystalline 3C – SiC : Influence of stacking faults. *Phys. Rev. B*, **58**:9858–9862, Oct 1998.
- [27] M. Bechelany, A. Brioude, D. Cornu, G. Ferro, and P. Miele. A Raman Spectroscopy Study of Individual SiC Nanowires. *Advanced Functional Materials*, **17**(6):939–943.
- [28] LZ Liu, J Wang, XL Wu, TH Li, and Paul K Chu. Longitudinal optical phonon-plasmon coupling in luminescent 3C-SiC nanocrystal films. *Optics letters*, **35**(23):4024–4026, 2010.
- [29] Hua Yang Sun, Siou-Cheng Lien, Zhi Ren Qiu, Hong Chao Wang, Ting Mei, Chee Wee Liu, and Zhe Chuan Feng. Temperature dependence of Raman scattering in bulk 4H-SiC with different carrier concentration. *Opt. Express*, **21**(22):26475–26482, Nov 2013.
- [30] Shuai Chen, Lingyu Wan, Deng Xie, Zhi Ren Qiu, Xiaodong Jiang, Chin-Che Tin, and Zhe Chuan Feng. Adducing crystalline features from Raman scattering studies of cubic SiC using different excitation wavelengths. *Journal of Physics D: Applied Physics*, **50**(11):115102, 2017.
- [31] Yan Peng, Xiaobo Hu, Xiangang Xu, Xiufang Chen, Juan Peng, Jisheng Han, and Sima Dimitrijević. Temperature and doping dependence of the Raman scattering in 4H-SiC. *Opt. Mater. Express*, **6**(9):2725–2733, Sep 2016.
- [32] Yutian Wang, Lin Li, Slawomir Prucnal, Xuliang Chen, Wei Tong, Zhaorong Yang, Frans Munnik, Kay Potzger, Wolfgang Skorupa, Sibylle Gemming, Manfred Helm, and Shengqiang Zhou. Disentangling defect-induced ferromagnetism in SiC. *Phys. Rev. B*, **89**:014417, Jan 2014.
- [33] A. Kaminski and S. Das Sarma. Polaron Percolation in Diluted Magnetic Semiconductors. *Phys. Rev. Lett.*, **88**:247202, May 2002.
- [34] C. Chiorescu, J. L. Cohn, and J. J. Neumeier. Impurity conduction and magnetic polarons in antiferromagnetic oxides. *Phys. Rev. B*, **76**:020404, Jul 2007.
- [35] J. M. D. Coey, M. Venkatesan, and C. B. Fitzgerald. Donor impurity band exchange in dilute ferromagnetic oxides. *Nature Materials*, **4**:173–179, 01 2005.
- [36] Bappaditya Pal and P. K. Giri. High temperature ferromagnetism and optical properties of Co doped ZnO nanoparticles. *Journal of Applied Physics*, **108**(8):084322, 2010.
- [37] R. Podila, W. Queen, A. Nath, Jeverson T. Arantes, Aline L. Schoenhalz, A. Fazzio, Gustavo M. Dalpian, J. He, Shiou J. Hwu, Malcolm J. Skove, and Apparao M. Rao. Origin of FM Ordering in Pristine Micro- and Nanostructured ZnO. *Nano Letters*, **10**(4):1383–1386, 2010. PMID: 20196539.
- [38] Yutian Wang, Yu Liu, Elke Wendler, René Hübner, Wolfgang Anwand, Gang Wang, Xuliang Chen, Wei Tong, Zhaorong Yang, Frans Munnik, Gregor Bukalis, Xiaolong Chen, Sibylle Gemming, Manfred Helm, and Shengqiang Zhou. Defect-induced magnetism in SiC: Interplay between ferromagnetism and paramagnetism. *Phys. Rev. B*, **92**:174409, Nov 2015.